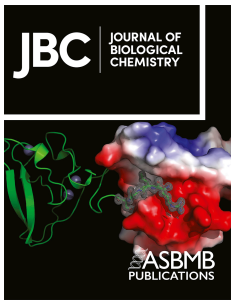

Bi-directional epithelial-mesenchymal crosstalk provides self-sustaining pro-fibrotic signals in pulmonary fibrosis

Liudi Yao, Yilu Zhou, Juanjuan Li, Leanne Wickens, Franco Conforti, Anna Rattu, Fathima Maneesha Ibrahim, Aiman Alzetani, Ben G. Marshall, Sophie V. Fletcher, David Hancock, Tim Wallis, Julian Downward, Rob M. Ewing, Luca Richeldi, Paul Skipp, Donna E. Davies, Mark G. Jones, Yihua Wang

PII: S0021-9258(21)00899-1

DOI: https://doi.org/10.1016/j.jbc.2021.101096

Reference: JBC 101096

To appear in: *Journal of Biological Chemistry*

Received Date: 10 June 2021

Revised Date: 6 August 2021

Accepted Date: 17 August 2021

Please cite this article as: Yao L, Zhou Y, Li J, Wickens L, Conforti F, Rattu A, Ibrahim FM, Alzetani A, Marshall BG, Fletcher SV, Hancock D, Wallis T, Downward J, Ewing RM, Richeldi L, Skipp P, Davies DE, Jones MG, Wang Y, Bi-directional epithelial-mesenchymal crosstalk provides self-sustaining pro-fibrotic signals in pulmonary fibrosis, *Journal of Biological Chemistry* (2021), doi: https://doi.org/10.1016/j.jbc.2021.101096.

Bi-directional epithelial-mesenchymal crosstalk provides self-sustaining pro-fibrotic signals in pulmonary fibrosis

Liudi Yao[1], Yilu Zhou[1,2], Juanjuan Li[1], Leanne Wickens[1,3], Franco Conforti[4,5], Anna Rattu[1], Fathima Maneesha Ibrahim[1], Aiman Alzetani[5,6], Ben G. Marshall[5,6], Sophie V. Fletcher[5,6], David Hancock[7], Tim Wallis[5,6], Julian Downward[7], Rob M. Ewing[1,2], Luca Richeldi[4,5,8], Paul Skipp[1,2,3], Donna E. Davies[2,4,5], Mark G. Jones[2,4,5,9], and Yihua Wang[1,2,5,9]

[1]Biological Sciences, Faculty of Environmental and Life Sciences, University of Southampton, Southampton SO17 1BJ, UK. [2]Institute for Life Sciences, University of Southampton, Southampton SO17 1BJ, UK. [3]Centre for Proteomic Research, Institute for Life Sciences, University of Southampton, Southampton SO17 1BJ, UK. [4]Clinical and Experimental Sciences, Faculty of Medicine, University of Southampton, Southampton SO16 6YD, UK. [5]NIHR Southampton Biomedical Research Centre, University Hospital Southampton, Southampton SO16 6YD, UK. [6]University Hospital Southampton, Southampton SO16 6YD, UK. [7]Oncogene Biology, The Francis Crick Institute, London NW1 1AT, UK. [8]Unità Operativa Complessa di Pneumologia, Università Cattolica del Sacro Cuore, Fondazione Policlinico A. Gemelli, Rome, Italy. [9]Correspondence should be addressed to YW (e-mail: yihua.wang@soton.ac.uk) or MGJ (mark.jones@soton.ac.uk).

Running title: Epithelial-mesenchymal crosstalk in pulmonary fibrosis

Keywords: Pulmonary fibrosis; epithelial-mesenchymal transition; ZEB1; SPARC; EGFR; RAS; TGF-β.

Abstract

Idiopathic pulmonary fibrosis (IPF) is the prototypic progressive fibrotic lung disease with a median survival of 2-4 years. Injury to and/or dysfunction of the alveolar epithelium is strongly implicated in IPF disease initiation, but the factors that determine whether fibrosis progresses rather than normal tissue repair occurs remain poorly understood. We previously demonstrated that ZEB1-mediated epithelial-mesenchymal transition (EMT) in human alveolar epithelial type II (ATII) cells augments TGF-β-induced profibrogenic responses in underlying lung fibroblasts via paracrine signalling. Here we investigated bi-directional epithelial-mesenchymal crosstalk and its potential to drive fibrosis progression. RNA sequencing (RNA-seq) of lung fibroblasts exposed to conditioned media from ATII cells undergoing RAS-induced EMT identified many differentially expressed genes including those involved in cell migration and extracellular matrix (ECM) regulation. We confirmed that paracrine signalling between RAS-activated ATII cells and fibroblasts augmented fibroblast recruitment and demonstrated that this involved a ZEB1-tissue plasminogen activator (tPA) axis. In a reciprocal fashion, paracrine signalling from TGF-β-activated lung fibroblasts or IPF fibroblasts induced RAS activation in ATII cells, at least partially through the secreted protein, SPARC, which may signal via the epithelial growth factor receptor (EGFR) via EGF-like (EGFL) repeats. Together, these data identify that aberrant bi-directional epithelial-mesenchymal crosstalk in IPF drives a chronic feedback loop that maintains a wound-healing phenotype and provides self-sustaining pro-fibrotic signals.

Introduction

Fibrotic diseases are a major cause of morbidity and mortality worldwide, and their prevalence is increasing with an ageing population (1). Development of effective treatments for progressive fibrosis is considered one of the most challenging tasks in modern medicine.

Our studies focus within the lung upon fibrotic interstitial lung diseases (ILDs), a diverse group of conditions that affect the space between the alveolar epithelium and the capillary endothelium to cause varying degrees of inflammation and fibrosis. Once considered rare, epidemiologic investigations have found them to be more common than previously recognized, with interstitial lung abnormalities detected in 7% of the general population (age > 50) resulting in an increase all-cause mortality (hazard ratio 2.7) (2). Idiopathic pulmonary fibrosis (IPF) is the prototypic chronic progressive fibrotic ILD, affecting 5 million people worldwide (3). Like many fibrotic disorders, IPF is characterized by enhanced deposition and remodelling of the extracellular matrix (ECM). This leads to decreased lung compliance, disrupted gas exchange, and ultimately respiratory failure and death. Median survival from diagnosis is 2-4 years and approved therapies only slow disease progression, so there is a significant unmet need.

An over-exuberant wound healing response is regarded as a canonical cause of organ fibrosis (4). Abnormal wound healing may occur as a consequence of multiple stimuli, including infections, chemical exposures, and physical injuries (5,6). Whilst injury to and/or dysfunction of the alveolar epithelium is strongly implicated in IPF disease initiation, the factors that determine whether fibrosis progresses rather than normal tissue repair occurs remain poorly understood.

In this study, we identify that aberrant bi-directional epithelial-mesenchymal crosstalk provides self-sustaining activation signals driving disease progression in pulmonary fibrosis. Building on our previous report (7), we provide evidence that alveolar epithelial type II (ATII) cells undergoing RAS-induced epithelial-mesenchymal transition (EMT) utilize a ZEB1-tissue plasminogen activator (tPA) axis to provide paracrine signals that augment fibroblast

recruitment and activation. In reciprocal paracrine signalling, TGF-β-activated fibroblasts or IPF fibroblasts induce RAS activation in ATII cells, which is at least partially driven by secreted protein acidic and rich in cysteine (SPARC). These findings support the concept that aberrant bi-directional epithelial-mesenchymal crosstalk contributes to the development of a profibrogenic microenvironment in which a chronic wound healing response leads to interstitial lung fibrosis.

Results

Global transcriptomic changes in fibroblasts exposed to conditioned media from RAS-activated ATII cells identify multiple processes including cell migration.

We previously reported that RAS-induced EMT in the human ATII cell line, ATII$^{ER:KRASV12}$ (in which RAS activation can be induced by 4-hydroxytamoxifen, 4-OHT) resulted in production of paracrine factors that augmented TGF-β-induced profibrogenic responses in lung fibroblasts (7). To determine if, and how, fibroblasts responded to epithelial signals in the absence of profibrogenic TGF-β signalling, we characterized the global transcriptomic changes in MRC5 lung fibroblasts exposed to conditioned media (CM) from control or RAS-induced ATII cells by performing RNA sequencing (RNA-seq).

Genes with a false discovery rate (FDR) adjusted *P* value less than 0.05 were considered as differentially expressed genes (DEGs). In total, 966 DEGs were identified, including 491 up-regulated (Supplementary Table 1) and 475 down-regulated (Supplementary Table 2). We then performed gene ontology (GO) enrichment analysis of the identified DEGs using PANTHER (8). The results were grouped into molecular function (MF), biological process (BP), and cellular component (CC). Interestingly, several IPF-related pathological terms were identified, including ECM and collagen, cell migration, and response to cytokine growth factor inflammatory stimulus which included TGF-β receptor signalling (FDR < 0.05; Fig. 1a; Supplementary Fig. S1; Supplementary Tables 3 and 4). Of these, cell migration and collagen containing extracellular matrix were among the top 10 ranked GO terms from the biological process category (Fig. 1b). These results extend our previous report (7) by demonstrating that CM from RAS-activated ATII cells regulates the expression of many genes that augment fibroblast activation and migration independent of exogenous TGF-β. Of note, under these conditions, we did not see changes in expression of *ACTA2*, encoding α-smooth muscle actin (α-SMA) (adjusted *P* value equals 0.289), suggesting that the fibroblasts did not adopt a myofibroblast phenotype under the conditions tested.

The effect of CM from RAS-induced ATII cells on genes controlling cell migration was further demonstrated using gene set variation analysis (GSVA) with a gene list from GO:0010763 (positive regulation of fibroblast migration); the GSVA score calculated based on this gene list was higher in MRC5 cells incubated with CM from 4-OHT-treated *vs.* control ATII$^{ER:KRASV12}$ cells ($P < 0.05$; Fig. 2a). To validate this finding on cell migration, scratch wound assays were performed using MRC5 or IPF fibroblasts (IPFFs) treated with CM from control or 4-OHT-activated ATII$^{ER:KRASV12}$ cells. Twenty-four hours after the scratch wound, IPFFs treated with CM from 4-OHT-activated ATII cells almost filled all the gaps, whereas the wound in the control cells was still open ($P < 0.01$; Fig. 2b). Similar results were obtained using MRC5 lung fibroblasts (Supplementary Fig. S2a). Under the same conditions, CM from RAS-activated ATII cells did not affect the cell viability in MRC5 (Supplementary Fig. S2b). In addition, in a transwell migration assay, a 3.5-fold increase in migration was detected using MRC5 lung fibroblasts treated with CM from 4-OHT-activated ATII$^{ER:KRASV12}$ cells compared with those treated with CM from control cells over a 24-hour period ($P < 0.001$; Fig. 2c). Together, these results demonstrate that RAS-activated ATII cells augment fibroblast migration via paracrine signalling.

RAS-activated ATII cells augment fibroblast migration via paracrine signalling, in which ZEB1 and tissue plasminogen activator are key regulators.

As we previously demonstrated that ZEB1 and its transcriptional target, tissue plasminogen activator (tPA, encoded by *PLAT* gene) are key regulators of epithelial-mesenchymal crosstalk (7), we hypothesized that these two proteins may also control the ability of RAS-activated ATII cells to promote migration and recruit fibroblasts by paracrine signalling. First, we depleted *ZEB1* in ATII$^{ER:KRASV12}$ cells via RNA interference (RNAi) (Supplementary Fig. S3a). We found that this completely abolished the pro-migratory effects of CM from RAS-activated ATII

cells on lung fibroblasts in both wound healing assay ($P > 0.05$; Fig. 3a and Supplementary Fig. S3b) and transwell migration assay ($P > 0.05$; Fig. 3b). Next, we determined whether tPA was a key paracrine regulator of fibroblast migration. Recombinant tPA treatment significantly enhanced fibroblast migration ($P < 0.0001$; Supplementary Fig. S3c). Similar to *ZEB1*, CM was collected from control or *PLAT*-depleted $ATII^{ER:KRASV12}$ cells treated without or with 4-OHT (Supplementary Fig. S3d and e). As expected, RAS-activated ATII cells augmented fibroblast migration in both wound healing assay ($P < 0.0001$; Fig. 3a and Supplementary Fig. S3f) and transwell migration assay ($P < 0.0001$; Fig. 3b) whereas under the same conditions, depletion of *PLAT* in $ATII^{ER:KRASV12}$ cells completely abolished the pro-migratory effects of CM from RAS-activated ATII cells on lung fibroblasts ($P > 0.05$; Fig. 3a and b; Supplementary Fig. S3f). Taken together, these data highlight the importance of ZEB1 and tPA as key regulators of epithelial-mesenchymal crosstalk to promote fibroblast recruitment, as well as fibroblast activation, as demonstrated previously (7) (Fig. 3c).

TGF-β-activated fibroblasts or IPF fibroblasts induce RAS activation in ATII cells.

Our current and previous (7) findings suggest that a ZEB1-tPA axis is involved in the paracrine signalling between RAS-activated ATII cells and fibroblasts to augment not only their recruitment but also their activation in the presence of TGF-β. To explore whether this epithelial-mesenchymal crosstalk was bi-directional, we investigated the effect of the activated fibroblasts on the alveolar epithelium. First, MRC5 lung fibroblasts were left untreated or treated with TGF-β (Supplementary Fig. S4a) to induce myofibroblast differentiation, as measured using the myofibroblast marker, α-SMA. An overall increase in α-SMA protein expression manifested after 24 hours of TGF-β treatment, with maximal induction being observed by western blot at 48 hours post-TGF-β treatment (Supplementary Fig. S4b). To eliminate the direct effect of exogenous TGF-β in CM collected from fibroblasts on ATII cells,

fibroblast cultures were placed in fresh medium without TGF-β for another 24 hours before CM was harvested (Supplementary Fig. S4a; group "48 h+, 24 h-"). As shown in Supplementary Fig. S4b, fibroblast differentiation into myofibroblasts was maintained under these conditions, evidenced by a comparable level of α-SMA protein level. We then treated ATII cells with CM from control or TGF-β-activated MRC5 cells (Supplementary Fig. S4c). Western blot analysis suggested that RAS signalling was activated upon treatment with CM from TGF-β-activated fibroblasts, reflected by significant increases in phosphorylation of AKT and ERK (Supplementary Fig. S4d). Of note, TGF-β-activated fibroblast CM also increased ZEB1 expression in ATII cells (Supplementary Fig. S4d). Since it has been reported that IPF-fibroblasts (IPFFs) have a higher level of autocrine TGF-β activation (9), we next compared the effects of CM from normal human lung fibroblasts (NHLFs) or IPFFs on ATII cells. We found RAS-ZEB1 signalling was significantly higher upon treatment with CM from IPFFs, reflected by significantly higher increases in phosphorylation of AKT and ERK levels ($P < 0.05$; Fig. 4a and b) as well as *ZEB1* ($P < 0.01$; Fig. 4c) and *PLAT* (tPA) expressions ($P < 0.01$; Fig. 4d). Together, these results suggest that signalling occurs between fibroblasts and ATII cells leading to RAS activation and induction of ZEB1, and that this effect is augmented by CM from fibroblasts that have been differentiated into myofibroblasts by TGF-β or by CM from IPFFs independently of exogenous TGF-β.

SPARC, a TGF-β-induced secreted protein, is highly expressed in IPF.

As CM derived from TGF-β-activated fibroblasts or IPFFs induced RAS signaling in ATII cells, we next investigated which secreted factors from activated fibroblasts were responsible for this effect. By performing quantitative proteomic analysis of the CM from control or TGF-β-treated MRC5 cells, we identified 15 secreted proteins whose levels were up-regulated upon TGF-β treatment (Table 1; Supplementary Tables 5 and 6). Of these, SPARC was among the

top candidates (Fig. 5a; Table 1), suggesting a potential regulatory role of SPARC in mesenchymal-epithelial crosstalk driven by TGF-β. This was further validated in a publicly available dataset (GSE139963) (10), in which RNA-seq was performed in human lung fibroblasts treated with or without TGF-β. Potential TGF-β-induced secreted proteins were identified by overlapping the up-regulated genes with a list of secreted proteins (predicted) from Human Protein Atlas (https://www.proteinatlas.org/humanproteome/tissue/secretome). We identified 116 predicted secreted proteins that were significantly elevated (FDR adjusted *P* value < 0.05 and Log_2[FoldChange] (Log_2[FC]) > 1) in TGF-β-treated lung fibroblasts compared to controls (Supplementary Fig. S5; Supplementary Table 7) and the expression of SPARC was increased by over 3-fold ($P < 0.001$) (Fig. 5b; Table 1; Supplementary Fig. S5b; Supplementary Table 7). The importance of SPARC in IPF pathogenesis was further confirmed in other datasets. In dataset GSE92592 (11), SPARC levels are increased in IPF tissues compared to control lungs ($P < 0.01$; Fig. 5c; Table 1), consistent with our recent report (12). Further analysis of GSE99621 (13) showed that SPARC expression is increased not only in scarred but also in those macroscopically unaffected (normal-appearing) regions of IPF lung ($P < 0.05$; Fig. 5d; Table 1). In addition, we confirmed a significantly enhanced secretion of SPARC in CM from IPFFs *vs.* NHLFs by western blotting ($P < 0.001$; Fig. 5e). Therefore, these data suggested that SPARC is induced as an early response to fibroblast activation and that it may be associated with IPF disease progression.

SPARC is a key fibroblast-derived paracrine regulator of RAS activation in ATII cells.

We recently reported that paracrine SPARC signalling from IPF fibroblasts dysregulates alveolar epithelial barrier integrity (12). We therefore hypothesized that SPARC might also mediate RAS activation in ATII cells during fibroblast-epithelial crosstalk. To test this hypothesis, ATII cells were exposed to CM harvested from control or *SPARC*-depleted NHLFs

treated without or with TGF-β (Supplementary Fig. S6a). As expected, we detected enhanced expression (Supplementary Fig. S6b) and secretion (Supplementary Fig. S6c) of SPARC from TGF-β-activated NHLFs compared to controls and this was abolished using RNAi. When the CM was applied to ATII cells, CM from TGF-β-activated fibroblasts induced RAS activation, as evidenced by increases of phosphorylation in both AKT and ERK, whereas depletion of *SPARC* completely abolished the effects of CM from TGF-β-activated fibroblasts on ATII cells (Supplementary Fig. S6c). We then compared CM from IPFFs: consistent with our previous results, an increased SPARC secretion was detected in CM from IPFFs *vs.* NHLFs (Supplementary Fig. S6d). Furthermore, while RAS signalling in ATII cells was activated by treatment with CM from IPFFs, these effects were completely abolished upon *SPARC* depletion in IPFFs (Fig. 6a; Supplementary Fig. S6d), as evidenced by decreased phosphorylation of AKT and ERK levels (Fig. 6b; Supplementary Fig. S6d). Furthermore, human recombinant SPARC (hrSPARC) treatment alone was sufficient to induce EGFR activation in ATII cells, demonstrated by increased phosphorylation levels of EGFR and its downstream AKT and ERK phosphorylation levels (Fig. 6c). EGFR activation was accompanied by a significant increase in mRNA expression of *ZEB1* (Fig. 6c), and a reduction in *CDH1* (E-cadherin) (Supplementary Fig. S6e). Therefore, our results strongly suggest that SPARC is a critical paracrine regulator from activated lung fibroblasts that induces RAS activation in ATII cells (Fig. 6d).

Discussion

IPF is a chronic, progressive lung disease with limited therapeutic options (5,14). Abnormal wound healing responses appear to make major contributions to the scarring process, but the underlying pathological mechanisms are unclear. Similar to studies in kidney fibrosis (15), our findings support the concept that aberrant epithelial-mesenchymal crosstalk contributes to the development of interstitial lung fibrosis. Our studies are consistent with the establishment of a bi-directional profibrogenic positive feedback loop which maintains a chronic wound environment involving activated epithelial cells and fibroblasts that drive fibrosis progression rather than wound resolution (Fig. 7).

Epithelial cells undergo EMT in response to injury, allowing them to adopt a repair phenotype which involves signalling to other cell types including inflammatory cells and resident mesenchymal cells. We previously reported that ATII cells undergoing RAS-induced EMT secrete tPA to augment TGF-β-induced myofibroblast differentiation and that ZEB1 is a key regulator of this paracrine signalling (7). To investigate further whether fibroblasts can respond to epithelial-derived signals in the absence of TGF-β, we used RNA-seq to study the global transcriptomic changes in lung fibroblasts exposed to CM from ATII cells undergoing RAS-induced EMT. Using this unbiased approach, several potential mechanisms of relevance to IPF pathology were identified, including ECM and collagen, cell migration, cytokine binding, and inflammatory response which included changes in expression of genes associated with TGF-β receptor signalling pathways. While we observed upregulation of ECM and collagen genes including *COL3A1*, *COL4A6*, *COL14A1* and *COL18A1* in the transcriptomic dataset, we did not observe changes in expression of either *COL1A1*, the major interstitial collagen produced in response to TGF-β stimulation, or *ACTA2* which encodes alpha-smooth muscle actin, a marker of myofibroblast differentiation (Supplementary Table 1; GSE163908). This suggests that the magnitude of TGF-β receptor signalling caused by the epithelial-derived

CM was insufficient to drive differentiation of the fibroblasts into myofibroblasts. These findings are consistent with our previous studies (7) where exogenous TGF-β was required to drive myofibroblast differentiation. However, our observation of upregulation of genes associated with TGF-β receptor signalling and increased expression of many profibrotic genes in fibroblasts following exposure to CM from epithelial cells undergoing RAS-induced EMT may help explain why the CM augmented the effects of exogenous TGF-β that we observed previously (7).

Building on the strong gene expression signature for cell migration, we confirmed induction of a migratory phenotype in fibroblasts exposed to epithelial CM and demonstrated that this involved a ZEB1-tPA signalling axis, similar to that required for augmentation of TGF-β-induced myofibroblast differentiation (7). Fibroblasts from pulmonary fibrosis have altered pathological properties (16) including enhanced migration compared to fibroblasts from control lungs (17,18). In our studies, we found that CM produced by ATII cells undergoing RAS-induced EMT markedly induced fibroblast migration and recruitment. The importance of the ZEB1-tPA axis in this process was then confirmed, with their silencing abolishing the pro-migratory effects of CM from RAS-activated ATII cells on lung fibroblasts. We previously identified that ZEB1 is expressed in epithelial cells of thickened alveolar septae where ECM deposition is evident (7). This suggests that ZEB1 is induced as an early response to alveolar epithelial injury and that, by regulating tPA expression, ZEB1 may promote fibroblast recruitment and thereby increase their numbers in the wound site. Consistent with our findings, it has been reported that neutralizing antibodies against tPA inhibit fibroblast migration (19). Mechanistically, tPA has direct cellular effects by virtue of its ability to bind to the low-density lipoprotein (LDL) receptor-related protein-1 (LRP-1), triggering LRP-1 tyrosine phosphorylation and recruitment of β1-integrin signalling involving integrin-linked kinase (ILK) (20,21).

While the activation of the ZEB1-tPA axis may be a normal physiological response to injury, deregulation of this axis may sensitize the underlying fibroblasts to drive a pathological profibrogenic response (22). Consistent with this concept, in kidney studies microinjuries on renal epithelium have been proposed to create a profibrotic microenvironment via TGF-β or connective tissue growth factor (CTGF) (15,23), promoting the aggregation of myofibroblasts, and in return, myofibroblasts may enhance the apoptosis of epithelial cells by secreting reactive oxygen species (ROS) (24,25) or angiotensin II (ANG II) (26,27), so generating self-sustained pathological feedbacks. We used CM harvested from TGF-β activated fibroblasts or IPF fibroblasts, and found that both enhanced RAS activation and induction of ZEB1 in ATII cells via paracrine signalling. Moreover, we found that CM from IPF fibroblasts induced significantly more RAS activation and ZEB1 expression than normal fibroblasts in the absence of exogenous TGF-β, pointing to a pathological mechanism within the IPF fibroblast population. This finding may be explained by a previous report that autocrine TGF-β signalling is enhanced in IPF fibroblasts (9). Taken together, these data suggest that bi-directional epithelial-mesenchymal crosstalk may become dysregulated in IPF leading to fibrosis progression rather than wound resolution.

Using proteomics and bioinformatics, we were able to identify SPARC, secreted by TGF-β-activated fibroblasts, as a key paracrine regulator of RAS activation in ATII cells. SPARC, a cysteine-rich acidic matrix-associated protein, containing 3 EGFL (EGF-like) repeats, is required for the collagen in bone to become calcified but is also involved in ECM synthesis and promotion of changes to cell shape (28-32) (33) (34,35). Consistent with our recent findings (12), our analysis based on publicly available transcriptome datasets indicate that SPARC expression is increased not only in scarred regions but also in macroscopically unaffected (normal-appearing) regions of IPF lung tissue (11,13). This suggests that SPARC is induced as an early response to fibroblast activation. We found that while SPARC expression

can be induced by TGF-β in normal lung fibroblasts, it is aberrantly expressed by IPF fibroblasts and that it acts via a paracrine mechanism to mediate RAS activation in ATII cells. SPARC has been shown by several studies to be able to regulate ERK signalling (36-38), although the upstream mechanism remains to be elucidated. In this study, our results demonstrated that SPARC alone is sufficient to induce EGFR activation in ATII cells, suggesting that SPARC might signal via the EGFR similar to tenascin C (39-41) via their EGFL repeats (42). Together, we have provided strong evidence suggesting that in both TGF-β-activated healthy lung fibroblasts and IPF fibroblasts, paracrine SPARC signalling dysregulates alveolar epithelial barrier integrity (12) and activates EGFR/RAS signalling in ATII cells to maintain a chronic wound-healing phenotype.

In summary, we identify a mechanism whereby bi-directional epithelial-mesenchymal crosstalk results in self-sustaining activation of wound healing responses. This involves a ZEB1-tPA axis in ATII cells which contributes to paracrine signalling that supports recruitment of fibroblasts and augments TGF-β-induced fibrotic responses; in turn, the aberrant behaviour of IPF fibroblasts (or normal fibroblasts activated by high levels of TGF-β) promotes persistent alveolar epithelial activation via paracrine mediators including SPARC, which prevents resolution of normal epithelial repair responses and restoration of tissue homeostasis. Such a chronic wound environment may drive disease progression in pulmonary fibrosis (Fig. 7).

Methods

Lung tissue sampling. All human lung tissue samples for primary cell culture were approved by the Southampton and South West Hampshire and the Mid and South Buckinghamshire Local Research Ethics Committees, and all subjects gave written informed consent. The study abided by the Declaration of Helsinki principles. Clinically indicated IPF lung biopsy tissue samples and non-fibrotic control tissue samples (macroscopically normal lung sampled remote from a cancer site) were assessed as surplus to clinical diagnostic requirements. All IPF samples were from patients subsequently receiving a multidisciplinary diagnosis of IPF according to international consensus guidelines (43).

Cell culture, reagents, and transfections. Primary parenchymal lung fibroblast cultures were established from IPF or control lung tissues as described previously (7,44-46). MRC5 lung fibroblasts were obtained from the European Collection of Authenticated Cell Cultures (ECACC). Fibroblasts were cultured in Dulbecco's Modified Eagle's Medium (DMEM) supplemented with 10% fetal bovine serum (FBS), 50 units/ml penicillin, 50µg/ml streptomycin, 2mM L-glutamine, 1mM sodium pyruvate, and 1x non-essential amino acids (all from Life Technologies). $ATII^{ER:KRASV12}$ cells(7,46-48) were cultured in DCCM-1 (Biological Industries Ltd) supplemented with 10% new-born calf serum (NBCS) (Life Technologies), 1% penicillin, 1% streptomycin, and 1% L-glutamine (all from Life Technologies). All cells were kept at 37 °C and 5% CO_2. No mycoplasma contamination was detected in the cell lines used.

Short interfering RNA (siRNA) oligos against *ZEB1* (MU-006564-02-0002, Set of 4 Upgrade) and *PLAT* (tPA) (MU-005999-01-0002, Set of 4 Upgrade) and *SPARC* (L-003710-00-0005; M-003710-02-0005) were purchased from Dharmacon. Sequences are available from Dharmacon, or on request. As a negative control, we used siGENOME RISC-Free siRNA (Dharmacon, D-001220–01). $ATII^{ER:KRASV12}$ cells were transfected with the indicated siRNA

oligos at a final concentration of 35 nM using DharmaFECT 2 reagent (Dharmacon). Fibroblasts were transfected with the indicated siRNA oligos at the same concentration using Lipofectamine RNAiMAX reagent (Invitrogen). Recombinant tPA protein was from Bio-Techne and human recombinant SPARC (hrSPARC) from Peprotech.

RNA isolation, library construction, and sequencing. To identify global transcriptomic changes in fibroblasts exposed to conditioned media (CM) from RAS-activated ATII cells, RNA sequencing (RNA-seq) was performed in MRC5 cells treated with either CM from control or 4-OHT-activated ATII$^{ER:KRASV12}$ cells. In brief, total RNA was isolated using RNeasy mini kit (Qiagen) according to manufacturer's instructions and quantified using a Nanodrop Spectophotometer 2000c (Thermo Fisher Scientific). A total amount of 3 μg RNA per sample was used as input material for library construction. Sequencing libraries were generated using NEBNext® UltraTM RNA Library Prep Kit for Illumina® (NEB, Ipswich, Massachusetts, USA) following manufacturer's instruction. Libraries were pooled in equimolar and sequenced using the paired-end strategy (2 × 150) on the Illumina NovaSeq 6000 platform following the standard protocols (Novogene, UK).

RNA-seq data analysis. Three publicly available datasets (GSE139963 (10), GSE92592 (11), and GSE99621 (13)) were collected from GEO. GSE139963 was in GPL18573 platform, Illumina NextSeq 500 (Homo sapiens), which composed of human lung fibroblasts treated with PBS (Control) or TGF-β in triplicates. GSE92592 was in GPL11154 platform, Illumina HiSeq 2000 (Homo sapiens), which consisted of 20 IPF and 19 control lung samples. GSE99621 was in GPL16791 platform, Illumina HiSeq 2500 (Homo sapiens), which included 26 samples from indicated sections (8 from healthy lungs, 10 from IPF unaffected lung tissues, and 8 from IPF

scared areas). Quality control of GSE163908, GSE139963, GSE92592, and GSE99621 data was performed using FastQC (http://www.bioinformatics.babraham.ac.uk/projects/fastqc) and MultiQC(49). Trim Galore (https://github.com/FelixKrueger/TrimGalore) was used to trim adapters, reads with low quality (< 30), and short length (< 50 bp). RNA-seq reads were mapped to Human genome Ensembl GRCh38 using Hisat2(50) (version 2.1.0) with default codes. Sam files were transformed into bam files using samtools (51) (version 1.9). The read counts of each gene were summarized using featureCounts (52) (version 1.6.5). Raw read counts were imported into RStudio (version 3.6.1) and analyzed by using R package of DESeq2 (53) (version 1.26.0). Transcripts with low abundance (under 10 counts across all samples) were removed. Genes with false discovery rate (FDR) *P*-value less than 0.05 adjusted by using Benjamini–Hochberg (BH) method were considered as differentially expressed genes (DEGs).

Pathway enrichment analysis. Gene ontology (GO) enrichment analysis was generated through PANTHER (8) website (http://pantherdb.org/). REVIGO TreeMap was generated via an online tool available at http://revigo.irb.hr/ (54). Parameters were set as FDR < 0.05. Gene set variation analysis (GSVA) (55) was used to calculate pathway activity.

Western blot analysis. Western blot analysis was performed with lysates from cells with urea buffer (8 M Urea, 1 M Thiourea, 0.5% CHAPS, 50 mM DTT, and 24 mM Spermine). Primary antibodies were from: Cell Signalling Technology (α-SMA, 14968; Phospho-Smad2, 3104; β-tubulin, 86298; phospho-EGFR, 2234; phospho-AKT, 9271; phospho-ERK, 9101; AKT, 9272; ERK, 9102; EGFR, 4267), Santa Cruz (ZEB1, sc-25388; SPARC, sc-398419), and Millipore (tPA, 05-883). Signals were detected using an ECL detection system (GE Healthcare) or Odyssey imaging system (LI-COR), and evaluated by ImageJ 1.42q software (National Institutes of Health).

qRT-PCR. Real-time quantitative RT-PCR was performed using gene-specific primers (QuantiTect Primer Assays, Qiagen) for *ZEB1* (QT00008555), *PLAT* (tPA) (QT00075761), *CDH1* (E-cadherin) (QT00080143) or *ACTB* (β-actin) (QT01680476) with QuantiNova SYBR Green RT-PCR kits (Qiagen). Relative transcript levels of target genes were normalized to *ACTB* (β-actin).

Wound-healing migration assay. The wound-healing migration assays were done in serum-starved fibroblasts. Confluent monolayers of cells were wounded with a p20 pipette tip (time 0). Phase-contrast images were taken using an Olympus inverted microscope at time 0 hour or 24 hours after the scratch wound. Wound areas were evaluated by ImageJ 1.42q software (National Institutes of Health).

Transwell migration assay. For the Transwell migration assay, Transwell membranes (8-μm pore size, 6.5-mm diameter; Corning Costar, 3422) were used (46,56,57). The bottom chambers of the Transwell were filled with indicated conditioned media. The top chambers were seeded with 1.5×10^5 serum-starved fibroblasts per well. After 24 hours, the filters were fixed with 4% paraformaldehyde for 10 min at room temperature; subsequently, the cells on the upper side of the membrane were scraped with a cotton swab. Filters were stained with crystal violet for light microscopy. Images were taken using an Olympus inverted microscope and migratory cells were evaluated by ImageJ 1.42q software (National Institutes of Health).

Quantitative proteomic analysis of the fibroblasts secretome and data processing. Proteomic experiment was performed in 3 biological replicates. Serum-free conditioned media from MRC5 cells treated with or without TGF-β1 (10ng/ml, 48h) were enriched based upon

Strataclean resin (Agilent) and analyzed using LC-MSE (58), to provide estimates of absolute protein concentration with in-depth coverage. Raw data were analyzed and exported into a csv document. Normalization method for each data is first dividing by the sum of each sample, using proteins containing no missing data, then multiplying by 10,000 (7). Minimum values of each column after normalization were used as pseudo-counts to replace all the missing data, allowing for a complete statistical analysis (59). Differentially expressed proteins between 2 groups with $P < 0.05$ were identified as significant using a two-tailed, unpaired Student's t-test (details described in Supplementary Method).

Statistical analysis and repeatability of experiments. Each experiment was repeated at least twice. Data are presented as mean and s.d. (standard deviation), and compared with Two Sample *t*-test, Welch Two Sample *t*-test, Mann-Whitney *U* test or one-way ANOVA test if appropriate. $P < 0.05$ was considered statistically significant. All data analyses and graphs were done in RStudio (version 3.6.1) or GraphPad Prism (version 8.2.1). Codes are available upon request.

Data Availability. RNA-seq data have been deposited in the Gene Expression Omnibus (GEO) database (accession code GSE163908). The mass spectrometry proteomics data have been deposited to the ProteomeXchange Consortium via the PRIDE repository (60) with the dataset identifier PXD025821.

Acknowledgements

This project was supported by Medical Research Council (MR/S025480/1), an Academy of Medical Sciences/the Wellcome Trust Springboard Award [SBF002\1038], the Wessex Medical Trust, and AAIR Charity. LY was supported by China Scholarship Council. YZ was supported by an Institute for Life Sciences PhD Studentship. FC was supported by Medical Research Foundation [MRF-091-0003-RG-CONFO]. JD was supported by the Francis Crick Institute which receives its core funding from Cancer Research UK (FC001070), the UK Medical Research Council (FC001070), and the Wellcome Trust (FC001070). Instrumentation in the Centre for Proteomic Research is supported by the BBSRC [BM/M012387/1] and the Wessex Medical Trust. We thank Carine Fixmer, Maria Lane, Benjamin Johnson, and the nurses of the Southampton Biomedical Research Unit for their help in the collection of human samples, supported by the Wessex Clinical Research Network and the National Institute of Health Research, UK.

Conflict of interest

The authors declare that they have no relevant conflict of interest.

Table 1 List of secreted proteins in the conditioned media that are up-regulated upon TGF-β treatment in MRC5 cells identified by quantitative proteomic analysis and their expressions in GSE139963, GSE92592 and GSE99621.

	Secretome		**GSE139963**		**GSE92592**		**GSE99621**			
	TGF-β *vs.* Control		**TGF-β *vs.* Control**		**IPF *vs.* Control**		**IPF-Normal *vs.* Control**		**IPF-Scarred *vs.* Control**	
Protein	***P*-value**	**Log_2FC**	***FDR***	**Log_2FC**	***FDR***	**Log_2FC**	***FDR***	**Log_2FC**	***FDR***	**Log_2FC**
A2M	***1.08E-02***	5.44	***0.00E+00***	-3.74	***1.76E-08***	1.01	***2.45E-03***	0.80	2.16E-01	0.41
IGFBP3	***3.94E-04***	4.70	***1.22E-89***	6.14	***1.21E-04***	1.01	6.50E-01	0.20	7.33E-01	0.17
SERPINE2	***1.84E-03***	4.11	***0.00E+00***	3.85	***1.26E-15***	2.37	***6.26E-05***	1.53	***2.59E-04***	1.49
PXDN	***1.29E-04***	3.51	***5.92E-235***	1.63	***8.00E-05***	0.77	1.24E-01	0.40	***1.26E-03***	0.77
PGS1	***1.29E-03***	2.06	***8.44E-04***	-0.32	4.85E-01	-0.08	7.74E-02	-0.42	***2.16E-02***	-0.55
THBS1	***2.69E-02***	1.98	***0.00E+00***	2.02	***4.37E-02***	1.01	8.57E-01	-0.12	8.95E-01	-0.10
SPARC	***4.75E-02***	1.80	***0.00E+00***	1.76	***1.37E-04***	0.87	***4.58E-03***	0.89	***2.86E-04***	1.15
APOA1-AS	***2.43E-02***	1.79	2.02E-01	-0.37	***9.27E-08***	-1.54	***5.36E-07***	-2.51	***1.70E-05***	-2.31
COL4A2	***2.06E-02***	1.47	***0.00E+00***	2.98	***1.25E-04***	0.91	8.00E-01	0.14	2.54E-01	0.49
TGFBI	***1.20E-03***	1.41	***1.17E-221***	1.76	***5.91E-07***	0.90	***4.28E-03***	0.90	***2.50E-03***	0.99
MMP2	***3.99E-02***	1.11	***9.86E-108***	1.16	***9.10E-18***	2.04	***1.84E-13***	1.32	***3.05E-13***	1.38
FN1	***1.14E-03***	1.00	***0.00E+00***	1.76	5.86E-02	0.52	***2.56E-07***	1.04	***3.33E-09***	1.23
IGFBP7	***9.63E-04***	0.66	***3.29E-99***	1.74	***7.19E-09***	0.92	***6.31E-16***	1.42	***8.76E-20***	1.66
COL12A1	***4.19E-02***	0.51	6.97E-01	-0.04	***1.57E-02***	0.51	2.63E-01	0.37	3.94E-01	0.32
CYCS	***1.77E-03***	0.40	***6.29E-10***	0.52	2.62E-01	0.15	8.97E-01	0.05	8.84E-01	0.06

Numbers in ***bold-italics*** mean *P* values less than 0.05 and are statistically significant. FDR: false discovery rate. FC: Fold change.

References

1. Richeldi, L., Collard, H. R., and Jones, M. G. (2017) Idiopathic pulmonary fibrosis. *Lancet* **389**, 1941-1952
2. Putman, R. K., Hatabu, H., Araki, T., Gudmundsson, G., Gao, W., Nishino, M., Okajima, Y., Dupuis, J., Latourelle, J. C., Cho, M. H., El-Chemaly, S., Coxson, H. O., Celli, B. R., Fernandez, I. E., Zazueta, O. E., Ross, J. C., Harmouche, R., Estepar, R. S., Diaz, A. A., Sigurdsson, S., Gudmundsson, E. F., Eiriksdottir, G., Aspelund, T., Budoff, M. J., Kinney, G. L., Hokanson, J. E., Williams, M. C., Murchison, J. T., MacNee, W., Hoffmann, U., O'Donnell, C. J., Launer, L. J., Harrris, T. B., Gudnason, V., Silverman, E. K., O'Connor, G. T., Washko, G. R., Rosas, I. O., Hunninghake, G. M., Evaluation of, C. L. t. I. P. S. E. I., and Investigators, C. O. (2016) Association Between Interstitial Lung Abnormalities and All-Cause Mortality. *Jama* **315**, 672-681
3. Meltzer, E. B., and Noble, P. W. (2008) Idiopathic pulmonary fibrosis. *Orphanet journal of rare diseases* **3**, 8
4. Wynn, T. A. (2011) Integrating mechanisms of pulmonary fibrosis. *Journal of Experimental Medicine* **208**, 1339-1350
5. Richeldi, L., Collard, H. R., and Jones, M. G. (2017) Idiopathic pulmonary fibrosis. *The Lancet* **389**, 1941-1952
6. Wynn, T. A. (2007) Common and unique mechanisms regulate fibrosis in various fibroproliferative diseases. *The Journal of clinical investigation* **117**, 524-529
7. Yao, L., Conforti, F., Hill, C., Bell, J., Drawater, L., Li, J., Liu, D., Xiong, H., Alzetani, A., and Chee, S. J. (2019) Paracrine signalling during ZEB1-mediated epithelial–mesenchymal transition augments local myofibroblast differentiation in lung fibrosis. *Cell Death & Differentiation* **26**, 943-957
8. Mi, H., Muruganujan, A., Huang, X., Ebert, D., Mills, C., Guo, X., and Thomas, P. D. (2019) Protocol Update for large-scale genome and gene function analysis with the PANTHER classification system (v. 14.0). *Nature protocols* **14**, 703-721
9. Ghatak, S., Bogatkevich, G. S., Atnelishvili, I., Akter, T., Feghali-Bostwick, C., Hoffman, S., Fresco, V. M., Fuchs, J. C., Visconti, R. P., Markwald, R. R., Padhye, S. B., Silver, R. M., Hascall, V. C., and Misra, S. (2014) Overexpression of c-Met and CD44v6 receptors contributes to autocrine TGF-beta1 signaling in interstitial lung disease. *J Biol Chem* **289**, 7856-7872
10. Senavirathna, L. K., Huang, C., Pushparaj, S., Xu, D., and Liu, L. (2020) Hypoxia and transforming growth factor β1 regulation of long non-coding RNA transcriptomes in human pulmonary fibroblasts. *Physiological reports* **8**, e14343
11. Schafer, M. J., White, T. A., Iijima, K., Haak, A. J., Ligresti, G., Atkinson, E. J., Oberg, A. L., Birch, J., Salmonowicz, H., and Zhu, Y. (2017) Cellular senescence mediates fibrotic pulmonary disease. *Nature communications* **8**, 1-11
12. Conforti, F., Ridley, R., Brereton, C., Alzetani, A., Johnson, B., Marshall, B. G., Fletcher, S. V., Ottensmeier, C. H., Richeldi, L., and Skipp, P. (2020) Paracrine SPARC signaling dysregulates alveolar epithelial barrier integrity and function in lung fibrosis. *Cell Death Discovery* **6**, 1-11
13. Luzina, I. G., Salcedo, M. V., Rojas-Peña, M. L., Wyman, A. E., Galvin, J. R., Sachdeva, A., Clerman, A., Kim, J., Franks, T. J., and Britt, E. J. (2018) Transcriptomic evidence of immune activation in macroscopically normal-appearing and scarred lung tissues in idiopathic pulmonary fibrosis. *Cellular immunology* **325**, 1-13
14. Nici, L., Donner, C., Wouters, E., Zuwallack, R., Ambrosino, N., Bourbeau, J., Carone, M., Celli, B., Engelen, M., and Fahy, B. (2006) American thoracic society/European respiratory society statement on pulmonary rehabilitation. *American journal of respiratory and critical care medicine* **173**, 1390-1413
15. Prunotto, M., Budd, D. C., Gabbiani, G., Meier, M., Formentini, I., Hartmann, G., Pomposiello, S., and Moll, S. (2012) Epithelial–mesenchymal crosstalk alteration in kidney fibrosis. *The Journal of pathology* **228**, 131-147
16. Ramos, C., Montaño, M., García-Alvarez, J., Ruiz, V. c., Uhal, B. D., Selman, M., and Pardo, A. (2001) Fibroblasts from idiopathic pulmonary fibrosis and normal lungs differ in growth rate, apoptosis, and tissue inhibitor of metalloproteinases expression. *American journal of respiratory cell and molecular biology* **24**, 591-598

17. Pierce, E. M., Carpenter, K., Jakubzick, C., Kunkel, S. L., Evanoff, H., Flaherty, K. R., Martinez, F. J., Toews, G. B., and Hogaboam, C. M. (2007) Idiopathic pulmonary fibrosis fibroblasts migrate and proliferate to CC chemokine ligand 21. *European Respiratory Journal* **29**, 1082-1093
18. Suganuma, H., Sato, A., Tamura, R., and Chida, K. (1995) Enhanced migration of fibroblasts derived from lungs with fibrotic lesions. *Thorax* **50**, 984-989
19. Quax, P., Boxman, I., Van Kesteren, C., Verheijen, J., and Ponec, M. (1994) Plasminogen activators are involved in keratinocyte and fibroblast migration in wounded cultures in vitro. *Fibrinolysis* **8**, 221-228
20. Hu, K., Wu, C., Mars, W. M., and Liu, Y. (2007) Tissue-type plasminogen activator promotes murine myofibroblast activation through LDL receptor–related protein 1–mediated integrin signaling. *The Journal of clinical investigation* **117**, 3821-3832
21. Hu, K., Lin, L., Tan, X., Yang, J., Bu, G., Mars, W. M., and Liu, Y. (2008) tPA protects renal interstitial fibroblasts and myofibroblasts from apoptosis. *J Am Soc Nephrol* **19**, 503-514
22. Hill, C., Jones, M. G., Davies, D. E., and Wang, Y. (2019) Epithelial-mesenchymal transition contributes to pulmonary fibrosis via aberrant epithelial/fibroblastic cross-talk. *J Lung Health Dis* **3**, 31-35
23. Sakai, N., and Tager, A. M. (2013) Fibrosis of two: Epithelial cell-fibroblast interactions in pulmonary fibrosis. *Biochimica et Biophysica Acta (BBA)-Molecular Basis of Disease* **1832**, 911-921
24. Brezniceanu, M.-L., Lau, C. J., Godin, N., Chénier, I., Duclos, A., Éthier, J., Filep, J. G., Ingelfinger, J. R., Zhang, S.-L., and Chan, J. S. (2010) Reactive oxygen species promote caspase-12 expression and tubular apoptosis in diabetic nephropathy. *Journal of the American Society of Nephrology* **21**, 943-954
25. Kim, J., Seok, Y. M., Jung, K.-J., and Park, K. M. (2009) Reactive oxygen species/oxidative stress contributes to progression of kidney fibrosis following transient ischemic injury in mice. *American Journal of Physiology-Renal Physiology* **297**, F461-F470
26. Kim, S. H., Yu, M.-A., Ryu, E. S., Jang, Y.-H., and Kang, D.-H. (2012) Indoxyl sulfate-induced epithelial-to-mesenchymal transition and apoptosis of renal tubular cells as novel mechanisms of progression of renal disease. *Laboratory investigation* **92**, 488-498
27. Bhaskaran, M., Reddy, K., Radhakrishanan, N., Franki, N., Ding, G., and Singhal, P. C. (2003) Angiotensin II induces apoptosis in renal proximal tubular cells. *American Journal of Physiology-Renal Physiology* **284**, F955-F965
28. Demopoulos, K., Arvanitis, D., Vassilakis, D., Siafakas, N., and Spandidos, D. (2002) MYCL1, FHIT, SPARC, p16INK4 and TP53 genes associated to lung cancer in idiopathic pulmonary fibrosis. *Journal of cellular and molecular medicine* **6**, 215-222
29. Camino, A. M., Atorrasagasti, C., Maccio, D., Prada, F., Salvatierra, E., Rizzo, M., Alaniz, L., Aquino, J. B., Podhajcer, O. L., and Silva, M. (2008) Adenovirus-mediated inhibition of SPARC attenuates liver fibrosis in rats. *The journal of gene medicine* **10**, 993-1004
30. Frizell, E., Liu, S.-L., Abraham, A., Ozaki, I., Eghbali, M., Sage, E. H., and Zern, M. A. (1995) Expression of SPARC in normal and fibrotic livers. *Hepatology* **21**, 847-854
31. Hohenester, E., Maurer, P., and Timpl, R. (1997) Crystal structure of a pair of follistatin-like and EF-hand calcium-binding domains in BM-40. *The EMBO journal* **16**, 3778-3786
32. Sasaki, T., Hohenester, E., Göhring, W., and Timpl, R. (1998) Crystal structure and mapping by site-directed mutagenesis of the collagen-binding epitope of an activated form of BM-40/SPARC/osteonectin. *The EMBO journal* **17**, 1625-1634
33. Chang, W., Wei, K., Jacobs, S. S., Upadhyay, D., Weill, D., and Rosen, G. D. (2010) SPARC suppresses apoptosis of idiopathic pulmonary fibrosis fibroblasts through constitutive activation of β-catenin. *Journal of Biological Chemistry* **285**, 8196-8206
34. Said, N. A., Elmarakby, A. A., Imig, J. D., Fulton, D. J., and Motamed, K. (2008) SPARC ameliorates ovarian cancer-associated inflammation. *Neoplasia* **10**, 1092-1104
35. Alvarez, M. J., Prada, F., Salvatierra, E., Bravo, A. I., Lutzky, V. P., Carbone, C., Pitossi, F. J., Chuluyan, H. E., and Podhajcer, O. L. (2005) Secreted protein acidic and rich in cysteine produced by human melanoma cells modulates polymorphonuclear leukocyte recruitment and antitumor cytotoxic capacity. *Cancer research* **65**, 5123-5132
36. Liu, Y., Feng, Y., Wang, X., Yang, X., Hu, Y., Li, Y., Zhang, Q., Huang, Y., Shi, K., and Ran, C. (2020) SPARC Negatively Correlates With Prognosis After Transarterial Chemoembolization and Facilitates Proliferation and Metastasis of Hepatocellular Carcinoma via ERK/MMP Signaling Pathways. *Frontiers in Oncology* **10**, 813
37. Wang, Q., Yang, Q., Zhang, A., Kang, Z., Wang, Y., and Zhang, Z. (2019) Silencing of SPARC represses heterotopic ossification via inhibition of the MAPK signaling pathway. *Bioscience reports* **39**

38. Chang, C.-H., Yen, M.-C., Liao, S.-H., Hsu, Y.-L., Lai, C.-S., Chang, K.-P., and Hsu, Y.-L. (2017) Secreted protein acidic and rich in cysteine (SPARC) enhances cell proliferation, migration, and epithelial mesenchymal transition, and SPARC expression is associated with tumor grade in head and neck cancer. *International journal of molecular sciences* **18**, 1556
39. Iyer, A. K., Tran, K. T., Griffith, L., and Wells, A. (2008) Cell surface restriction of EGFR by a tenascin cytotactin-encoded EGF-like repeat is preferential for motility-related signaling. *J Cell Physiol* **214**, 504-512
40. Swindle, C. S., Tran, K. T., Johnson, T. D., Banerjee, P., Mayes, A. M., Griffith, L., and Wells, A. (2001) Epidermal growth factor (EGF)-like repeats of human tenascin-C as ligands for EGF receptor. *J Cell Biol* **154**, 459-468
41. Iyer, A. K., Tran, K. T., Borysenko, C. W., Cascio, M., Camacho, C. J., Blair, H. C., Bahar, I., and Wells, A. (2007) Tenascin cytotactin epidermal growth factor-like repeat binds epidermal growth factor receptor with low affinity. *J Cell Physiol* **211**, 748-758
42. Grahovac, J., and Wells, A. (2014) Matrikine and matricellular regulators of EGF receptor signaling on cancer cell migration and invasion. *Lab Invest* **94**, 31-40
43. Raghu, G., Remy-Jardin, M., Myers, J. L., Richeldi, L., Ryerson, C. J., Lederer, D. J., Behr, J., Cottin, V., Danoff, S. K., Morell, F., Flaherty, K. R., Wells, A., Martinez, F. J., Azuma, A., Bice, T. J., Bouros, D., Brown, K. K., Collard, H. R., Duggal, A., Galvin, L., Inoue, Y., Jenkins, R. G., Johkoh, T., Kazerooni, E. A., Kitaichi, M., Knight, S. L., Mansour, G., Nicholson, A. G., Pipavath, S. N. J., Buendia-Roldan, I., Selman, M., Travis, W. D., Walsh, S., Wilson, K. C., American Thoracic Society, E. R. S. J. R. S., and Latin American Thoracic, S. (2018) Diagnosis of Idiopathic Pulmonary Fibrosis. An Official ATS/ERS/JRS/ALAT Clinical Practice Guideline. *Am J Respir Crit Care Med* **198**, e44-e68
44. Conforti, F., Davies, E. R., Calderwood, C. J., Thatcher, T. H., Jones, M. G., Smart, D. E., Mahajan, S., Alzetani, A., Havelock, T., Maher, T. M., Molyneaux, P. L., Thorley, A. J., Tetley, T. D., Warner, J. A., Packham, G., Ganesan, A., Skipp, P. J., Marshall, B. J., Richeldi, L., Sime, P. J., O'Reilly, K. M. A., and Davies, D. E. (2017) The histone deacetylase inhibitor, romidepsin, as a potential treatment for pulmonary fibrosis. *Oncotarget* **8**, 48737-48754
45. Jones, M. G., Andriotis, O. G., Roberts, J. J., Lunn, K., Tear, V. J., Cao, L., Ask, K., Smart, D. E., Bonfanti, A., Johnson, P., Alzetani, A., Conforti, F., Doherty, R., Lai, C. Y., Johnson, B., Bourdakos, K. N., Fletcher, S. V., Marshall, B. G., Jogai, S., Brereton, C. J., Chee, S. J., Ottensmeier, C. H., Sime, P., Gauldie, J., Kolb, M., Mahajan, S., Fabre, A., Bhaskar, A., Jarolimek, W., Richeldi, L., O'Reilly, K. M., Monk, P. D., Thurner, P. J., and Davies, D. E. (2018) Nanoscale dysregulation of collagen structure-function disrupts mechano-homeostasis and mediates pulmonary fibrosis. *Elife* **7**
46. Hill, C., Li, J., Liu, D., Conforti, F., Brereton, C. J., Yao, L., Zhou, Y., Alzetani, A., Chee, S. J., Marshall, B. G., Fletcher, S. V., Hancock, D., Ottensmeier, C. H., Steele, A. J., Downward, J., Richeldi, L., Lu, X., Davies, D. E., Jones, M. G., and Wang, Y. (2019) Autophagy inhibition-mediated epithelial-mesenchymal transition augments local myofibroblast differentiation in pulmonary fibrosis. *Cell Death Dis* **10**, 591
47. Molina-Arcas, M., Hancock, D. C., Sheridan, C., Kumar, M. S., and Downward, J. (2013) Coordinate direct input of both KRAS and IGF1 receptor to activation of PI3 kinase in KRAS-mutant lung cancer. *Cancer Discov* **3**, 548-563
48. Coelho, M. A., de Carne Trecesson, S., Rana, S., Zecchin, D., Moore, C., Molina-Arcas, M., East, P., Spencer-Dene, B., Nye, E., Barnouin, K., Snijders, A. P., Lai, W. S., Blackshear, P. J., and Downward, J. (2017) Oncogenic RAS Signaling Promotes Tumor Immunoresistance by Stabilizing PD-L1 mRNA. *Immunity* **47**, 1083-1099 e1086
49. Ewels, P., Magnusson, M., Lundin, S., and Kaller, M. (2016) MultiQC: summarize analysis results for multiple tools and samples in a single report. *Bioinformatics* **32**, 3047-3048
50. Kim, D., Langmead, B., and Salzberg, S. L. (2015) HISAT: a fast spliced aligner with low memory requirements. *Nat Methods* **12**, 357-360
51. Li, H., Handsaker, B., Wysoker, A., Fennell, T., Ruan, J., Homer, N., Marth, G., Abecasis, G., Durbin, R., and Genome Project Data Processing, S. (2009) The Sequence Alignment/Map format and SAMtools. *Bioinformatics* **25**, 2078-2079
52. Liao, Y., Smyth, G. K., and Shi, W. (2014) featureCounts: an efficient general purpose program for assigning sequence reads to genomic features. *Bioinformatics* **30**, 923-930
53. Love, M. I., Huber, W., and Anders, S. (2014) Moderated estimation of fold change and dispersion for RNA-seq data with DESeq2. *Genome Biol* **15**, 550

54. Supek, F., Bosnjak, M., Skunca, N., and Smuc, T. (2011) REVIGO summarizes and visualizes long lists of gene ontology terms. *PLoS One* **6**, e21800
55. Hanzelmann, S., Castelo, R., and Guinney, J. (2013) GSVA: gene set variation analysis for microarray and RNA-seq data. *BMC Bioinformatics* **14**, 7
56. Wang, Y., Xiong, H., Liu, D., Hill, C., Ertay, A., Li, J., Zou, Y., Miller, P., White, E., Downward, J., Goldin, R. D., Yuan, X., and Lu, X. (2019) Autophagy inhibition specifically promotes epithelial-mesenchymal transition and invasion in RAS-mutated cancer cells. *Autophagy* **15**, 886-899
57. Liu, D., Ertay, A., Hill, C., Zhou, Y., Li, J., Zou, Y., Qiu, H., Yuan, X., Ewing, R. M., Lu, X., Xiong, H., and Wang, Y. (2020) ASPP1 deficiency promotes epithelial-mesenchymal transition, invasion and metastasis in colorectal cancer. *Cell Death Dis* **11**, 224
58. Silva, J. C., Gorenstein, M. V., Li, G.-Z., Vissers, J. P., and Geromanos, S. J. (2006) Absolute quantification of proteins by LCMSE: a virtue of parallel MS acquisition. *Molecular & Cellular Proteomics* **5**, 144-156
59. Wang, J., Li, L., Chen, T., Ma, J., Zhu, Y., Zhuang, J., and Chang, C. (2017) In-depth method assessments of differentially expressed protein detection for shotgun proteomics data with missing values. *Scientific reports* **7**, 1-8
60. Perez-Riverol, Y., Csordas, A., Bai, J., Bernal-Llinares, M., Hewapathirana, S., Kundu, D. J., Inuganti, A., Griss, J., Mayer, G., Eisenacher, M., Perez, E., Uszkoreit, J., Pfeuffer, J., Sachsenberg, T., Yilmaz, S., Tiwary, S., Cox, J., Audain, E., Walzer, M., Jarnuczak, A. F., Ternent, T., Brazma, A., and Vizcaino, J. A. (2019) The PRIDE database and related tools and resources in 2019: improving support for quantification data. *Nucleic Acids Res* **47**, D442-D450

Figure Legends

Fig. 1 Global transcriptomic changes in fibroblasts exposed to conditioned media from RAS-activated ATII cells. **a** REVIGO TreeMap showing Gene Ontology (GO) analysis of upregulated differentially expressed genes (DEGs) in MRC5 lung fibroblasts treated with conditioned media (CM) from 4-OHT-activated *vs.* control ATII$^{ER:KRASV12}$ cells. Common colours represent groupings based on parent GO terms, and each rectangle is proportional to the relative enrichment of the GO term compared to the whole genome. Genes with false discovery rate (FDR) < 0.05 were considered as DEGs (differentially expressed genes). **b** Scatter plot showing the top 10 enriched GO terms from 3 categories (biological process, cellular component and molecular function) according to rich factors. Rich factor is the percentage of DEGs enriched gene count in the given annotated GO terms. The sizes of circles represent gene counts, and the colours of circles represent the -Log_{10} of the adjusted *P*- values.

Fig. 2 RAS-activated ATII cells augment fibroblast migration via paracrine signalling. **a** Graph showing GSVA scores calculated based on a gene list from GO:0010763 (positive regulation of fibroblast migration) in MRC5 cells treated with CM from control or 4-OHT-activated ATII$^{ER:KRASV12}$ cells. Data are mean ± s.d. $n = 3$. $*P < 0.05$. **b** Scratch wound assay of fibroblasts treated with CM from control or 4-OHT-activated ATII$^{ER:KRASV12}$ cells. Representative images of IPF fibroblasts with the indicated treatments at time 0 or 24 hours after the scratch wound. Wounds have been artificially coloured red to aid visualization. Scale bar: 200 μm. Graph shows the areas of wounds evaluated with ImageJ, and data are mean ± s.d. $n = 3$. $**P < 0.01$. **c** Transwell migration assays in MRC5 fibroblasts with indicated treatment. Cells were stained with crystal violet. Scale bar: 100 μm. Data are mean ± s.d. $n = 3$. $***P < 0.001$.

Fig. 3 RAS-activated ATII cells augment fibroblast migration via paracrine signalling, in which ZEB1 and tissue plasminogen activator (tPA, encoded by gene *PLAT*) are key paracrine regulators. **a** Scratch wound assay of fibroblasts treated with CM from ATII$^{ER:KRASV12}$ cells with indicated treatment. Graph showing the areas of wounds evaluated with ImageJ, and data are mean ± s.d. $n = 3$. ****$P < 0.0001$. *n.s.* (not significant) $P > 0.05$. **b** Transwell migration assays in fibroblasts treated with CM from ATII$^{ER:KRASV12}$ cells with indicated treatment. Graph showing the percentage of positive staining of fibroblasts with indicated treatment evaluated with ImageJ, and data are mean ± s.d. $n = 3$. ****$P < 0.0001$. *n.s.* $P > 0.05$. **c** Diagram summarizing a key role of tPA secreted by RAS-activated ATII cells in augmenting fibroblast migration via paracrine signalling.

Fig. 4 IPF fibroblasts induce RAS activation in ATII cells via paracrine signalling. **a** Protein expression of phospho-AKT (p-AKT), AKT, phospho-ERK (p-ERK) and ERK in ATII cells treated with indicated CM from NHLFs (normal human lung fibroblasts) or IPFFs (IPF fibroblasts). β-tubulin was used as a loading control. **b** Graph showing protein levels of p-AKT or p-ERK in ATII cells treated with CM from NHLFs or IPFFs. Total AKT or ERK-normalized protein levels in ATII cells treated with CM from NHLFs were used to set the baseline value at unity. Data are mean ± s.d. $n = 3$. *$P < 0.05$. **c** and **d** Fold change in mRNA levels of *ZEB1* (**c**) or *PLAT* (**d**) in ATII cells treated with CM from NHLFs or IPFFs. β-actin-normalized mRNA levels in ATII cells treated with CM from NHLFs were used to set the baseline value at unity. Data are mean ± s.d. $n = 3$ samples per group. **$P < 0.01$.

Fig. 5 SPARC, a TGF-β-induced secreted protein, is highly expressed in IPF. **a** Quantitative secretome analysis identifies an increased level of SPARC in the conditioned media (CM) from TGF-β-treated MRC5 cells. Data are mean ± s.d. $n = 3$. * $P < 0.05$. **b** SPARC expression in

human lung fibroblasts treated with or without TGF-β (GSE139963). ***$P < 0.001$. **c** SPARC expression in lung tissues from healthy controls and IPF patients (GSE92592). ** $P < 0.01$. **d** SPARC expression in lung tissues from healthy controls and IPF samples with macroscopically normal-appearing (IPF-Normal) or scarred (IPF-Scarred) (GSE99621). * $P < 0.05$. **e** Protein expression of SPARC in conditioned media (CM) from NHLFs (normal human lung fibroblasts) or IPFFs (IPF fibroblasts). Ponceau S staining showing total protein levels. Graph showing SPARC protein levels in CM from NHLFs or IPFFs. Data are mean ± s.d. $n = 3$. ***$P < 0.001$.

Fig. 6 SPARC is a key fibroblast-derived paracrine regulator of RAS activation in ATII cells. **a** Protein expression of SPARC in CM from IPFFs (IPF fibroblasts) with indicated treatment. Ponceau S staining showing total protein levels. **b** Protein expression of phospho-AKT (p-AKT), AKT, phospho-ERK (p-ERK) and ERK in ATII cells treated with CM from IPFFs with indicated treatment. β-tubulin was used as a loading control. Total AKT or ERK-normalized protein levels in ATII cells treated with CM from control IPFFs were used to set the baseline value at unity. **c** Protein expression of phospho-EGFR (p-EGFR), EGFR, phospho-AKT (p-AKT), AKT, phospho-ERK (p-ERK) and ERK in ATII cells treated with or without human recombinant SPARC (hrSPARC). β-tubulin was used as a loading control. Total EGFR, AKT or ERK-normalized protein levels in control cells were used to set the baseline value at unity. Fold change in mRNA levels of *ZEB1* in ATII cells treated with or without hrSPARC. β-actin-normalized mRNA levels in control cells were used to set the baseline value at unity. Data are mean ± s.d. $n = 3$ samples per group. **$P < 0.01$. **d** Diagram summarizing SPARC as a key fibroblast-derived paracrine regulator of RAS activation in ATII cells.

Fig. 7 Diagram summarizing a critical role of bi-directional epithelial-mesenchymal crosstalk in pulmonary fibrosis (details provided in Discussion).

Figure 1

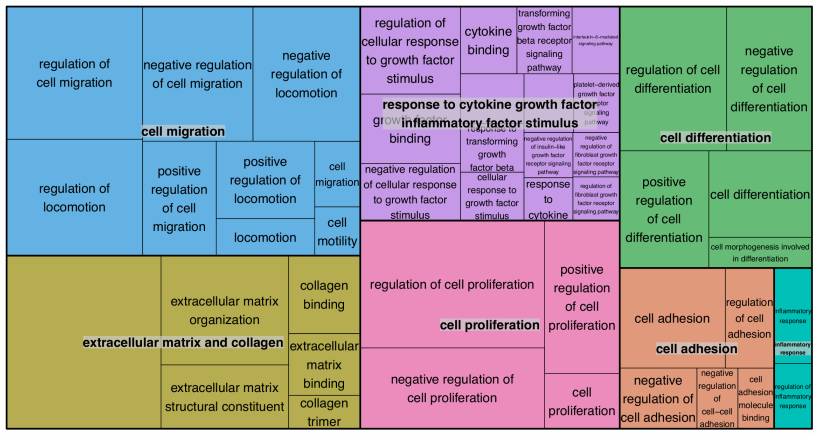

Figure 2

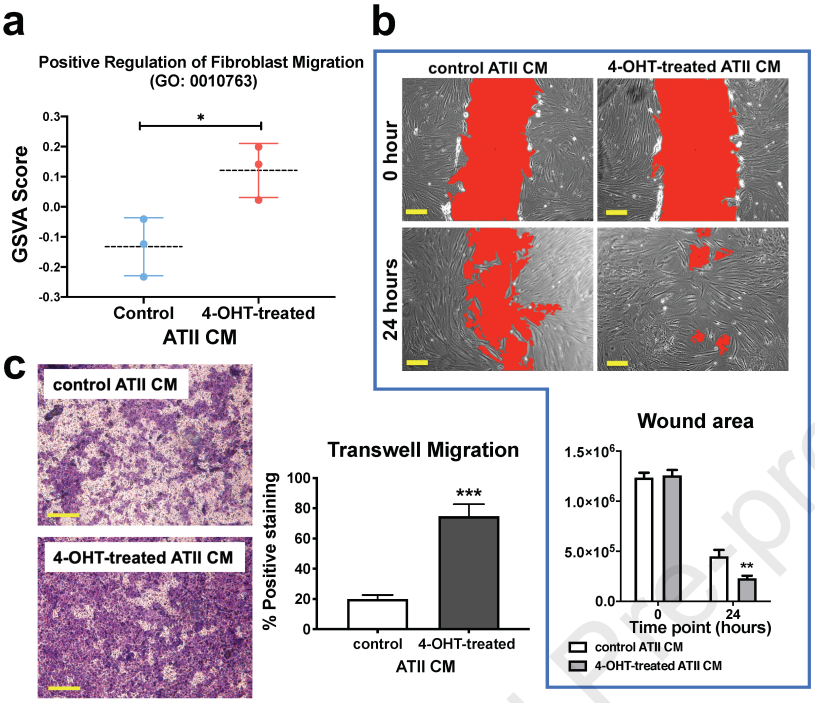

Figure 3

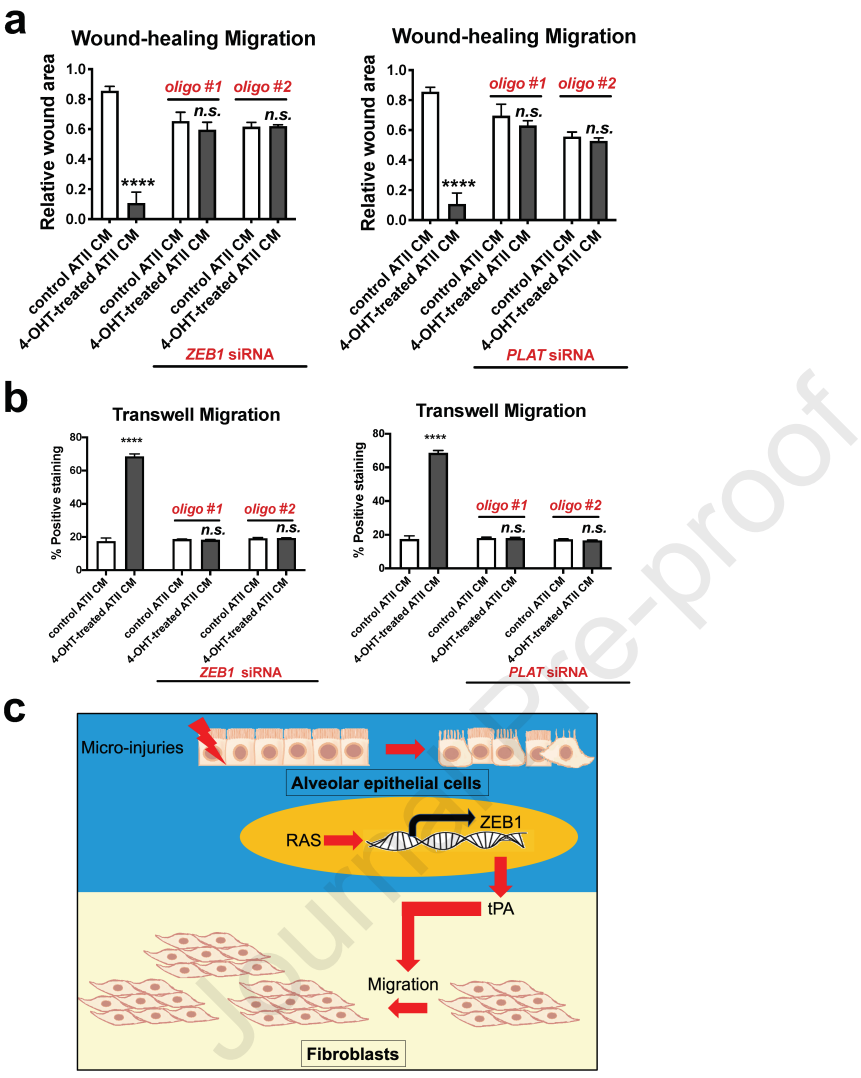

Figure 4

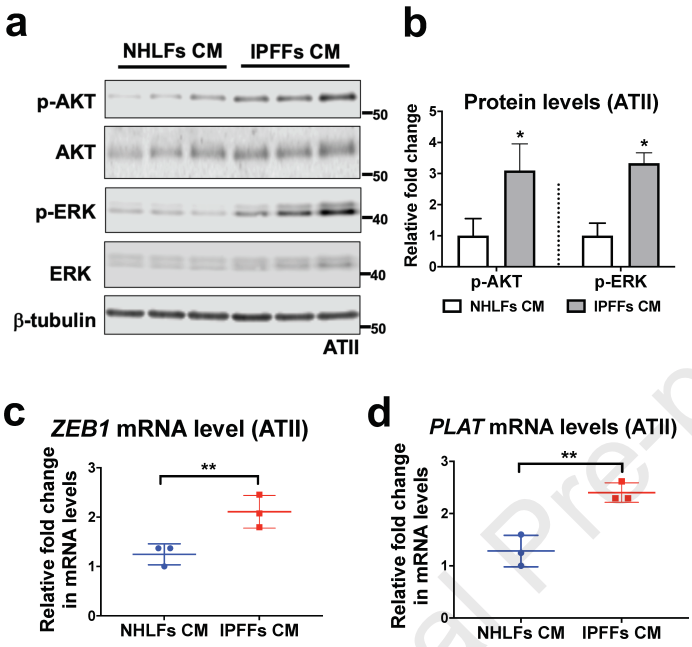

Figure 5

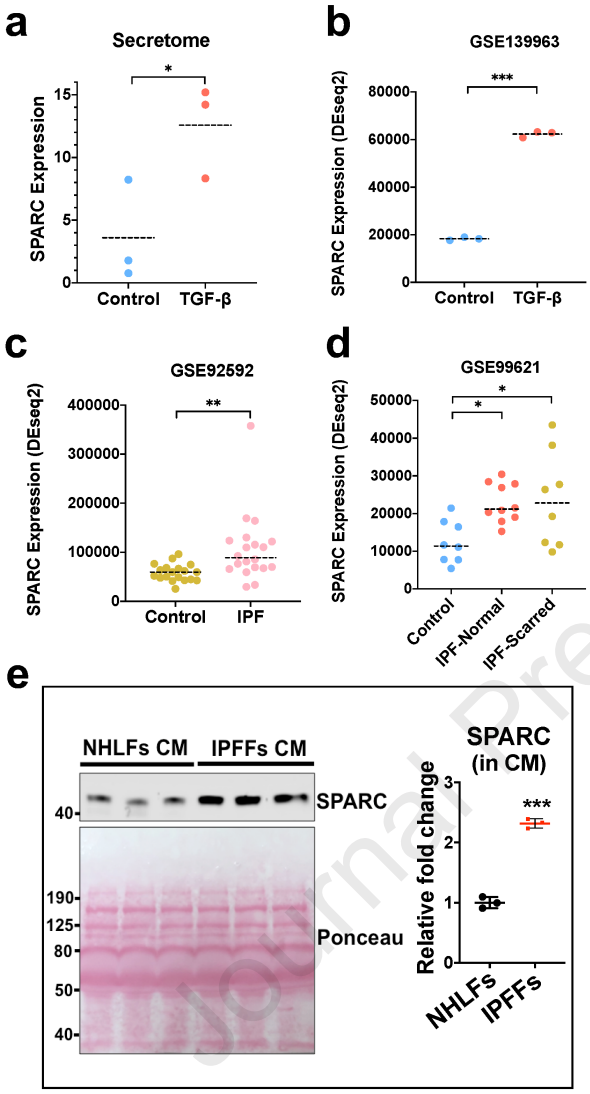

Figure 6

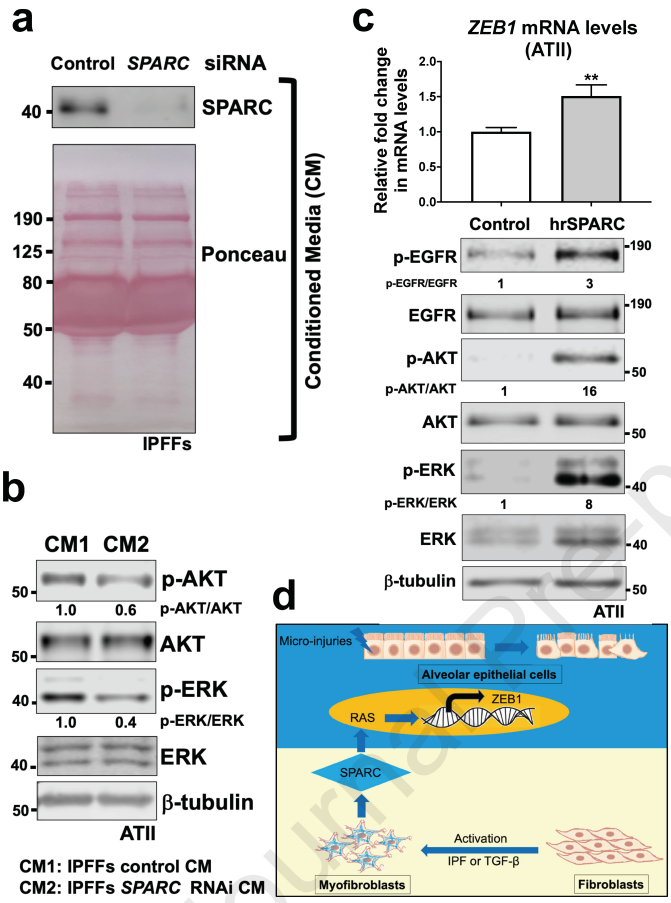

Figure 7